Geophys. J. R. astr. Soc. (1984) **78**, 1–17

High-frequency seismic radiation from a buried circular fault

P. Bernard *Laboratoire de Sismologie, associé au CNRS no. 195, Institut de Physique du Globe, Université Paris VI, 4, pl. Jussieu - Tour 14, 75230 Paris Cedex 05, France*

R. Madariaga *Laboratoire de Sismologie, associé au CNRS no. 195, Institut de Physique du Globe, Université Paris VI, 4, pl. Jussieu - Tour 14, 75230 Paris Cedex 05 and UER Sciences Physiques de la Terre, Université Paris VII, France*

Received 1983 March 28

Summary. We propose a simplified method for the calculation of near field accelerograms. It is based upon the hypothesis that, in the course of dynamic faulting, the dominating part of the seismic radiation is emitted by the rupture front. As the rupture moves smoothly it radiates continuously, generating the low-frequency part of the field. High-frequency waves are produced by jumps in the rupture velocity and abrupt changes in the stress intensity factor. The wave-front discontinuities created in this fashion are evaluated by asymptotic methods and may be propagated away from the source by ray theoretical methods. We apply our technique to the evaluation of asymptotic near field accelerograms for a circular fault buried in a half-space. The agreement with numerical accelerograms calculated by full-wave theory is very satisfactory. Two problems are given particular emphasis: (1) the phase shifts introduced by focusing and (2) a simpler method, based on dislocation theory, is proposed for the calculation of the radiation coefficients from a discontinuously moving rupture front.

1 Introduction

The modelling of synthetic accelerograms in the near field of a seismic source is of major importance for the prediction of strong ground motion and the evaluation of seismic risk. Synthetic records also provide a method to invert observed accelerograms to seismic source parameters, in particular to slip velocity on the fault. Several rather complex numerical methods have been proposed in the literature to calculate near field synthetics (Bouchon 1979, Heaton & Helmberger 1979, Hartzell & Helmberger 1982 among others).

All of these methods require laborious numerical integrations over a distribution of point double couple sources covering the whole fault plane. If one is interested only in high frequencies – wavelengths shorter than the distance to the observer and shorter than

the overall dimensions of the fault plane – it is possible to develop very efficient asymptotic methods for the simulation of accelerograms. These methods, proposed by Madariaga (1977) and Achenbach & Harris (1978), make use of a number of well-known results of the geometrical theory of diffraction to generalize the results obtained for simple 2-D fault models into three dimensions. Although the original papers dealt only with the simultaneous arrest of rupture around the periphery of the rupture front, we have recently extended these results to more general models of fracture arrest (Bernard & Madariaga 1984).

In this paper, we study the problem of focusing of stopping phases by the curvature of the rupture front. Focusing was considered by Achenbach & Harris (1978) although they did not include the phase shifts introduced into the stopping phase when it crosses the focal line. The $\pi/2$ phase shift (Hilbert transformation) introduced by focusing appears clearly in the time domain synthetic accelerograms calculated by Archuleta & Hartzell (1981) and Campillo (1983). It was when trying to interpret the different phases appearing in these synthetics that the Hilbert transformed waveforms were identified in the second stopping phases. We will demonstrate how to correct for these effects and show a number of calculations made for a simple model of a circular fault in a half-space. The calculations may be easily extended to more complex fault geometries including barriers and asperities (Madariaga 1983); and to more realistic geometries of the rupture front and asperity shape (Bernard & Madariaga 1984). We shall also present a simplified method for the approximate calculation of radiation coefficients from a crack edge. This method makes use of a moving dislocation approximation to the rupture front.

2 Geometrical and kinematic effects of fault curvature

The seismic radiation of high-frequency waves from a curved rupture front was studied by Madariaga (1977) and Achenbach & Harris (1978). These authors used Keller's (1962) geometrical theory of diffraction to extend their 2-D models of radiation to smoothly curved rupture fronts. Their results permit the calculation of the wavefront discontinuities or stopping phases radiated from a sudden change of velocity of a rupture front. They did not, however, consider the phase shift suffered by the stopping phases when they cross the focal line which appears when the radiation is observed from the concave side of a curved rupture front. This effect is very important in practical applications to the calculation of near field high-frequency accelerograms, since focusing by the rupture front may be a very common occurrence.

In order to illustrate the effect of focusing we will study a simple problem which contains all the geometrical effects we are interested in. We consider a circular ring source C, of radius a, embedded in an infinite, homogeneous medium of wave propagation velocity c. Each point on the circle C emits a simple spherical wave:

$$u(t, R) = \frac{\delta(t - R/c)}{R} \tag{1}$$

where R is the distance from the observation point P to the source and $\delta(t)$ is Dirac's delta function. Using Huyghen's principle we calculate the radiation from the circular ring integrating over all the point sources on the ring. The field at P is then:

$$C(t) = \frac{4aH(t - R_1/c)\,H(R_2/c - t)}{c\sqrt{t^2 - R_1^2/c^2}\sqrt{R_2^2/c^2 - t^2}} \tag{2}$$

where R_1 and R_2 are the minimum and maximum distances from P to the ring C, respectively (see Fig. 1a). The points A_1, A_2 and P are all on a plane perpendicular to the source

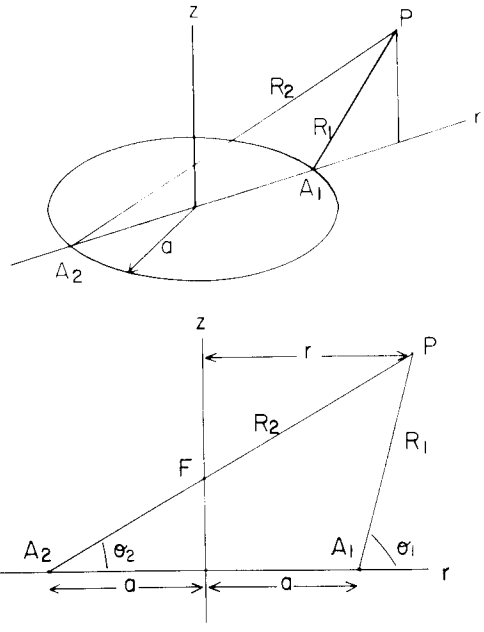

Figure 1. Geometry of the circular crack model used in the text. Rupture starts from the origin and spreads along the horizontal plane until the final radius a. At the observation P the main contributions to the accelerograms come from the stopping phases radiated by A_1 and A_2.

ring. The field $C(t)$ presents two singularities: the first at $t = R_1/C$ when motion at P starts, and the second at $t \simeq R_2/C$ when motion stops.

Near the starting front $t \simeq R_1/C$ we may approximate (2) by:

$$C_1(t) = \frac{2a}{\sqrt{R_2^2 - R_1^2}} \sqrt{2c/R_1}\, \frac{H(t - R_1/c)}{\sqrt{t - R_1/c}} \tag{3}$$

and $R_2^2 - R_1^2 = 4\,ar$, where r is the radial distance from P to the axis of the ring. Referring to Fig. 1 we may express r as:

$$r = a + R_1 \cos\theta_1 \tag{4}$$

so that (3) yields:

$$C_1(t) = \frac{1}{\sqrt{1 + R_1 \cos\vartheta_1/a}}\, L(t, R_1) \tag{5}$$

where:

$$L(t, R_1) = \sqrt{2c/R_1}\, \frac{H(t - R_1/c)}{\sqrt{t - R_1/c}} \tag{6}$$

is the radiation from a line source tangent to the ring C at the point A_1. This expression shows that the field near the first arrival from the circular source is equal to that of a local line source (6) corrected by the spreading factor $\sqrt{1 + R_1 \cos\vartheta_1/a}$. This is the same results obtained by Achenbach & Harris (1978) for a similar problem. Let us note, however, that on the concave side of the ring ($\cos\theta_1 < 0$), the solution (5) is not valid for:

$$R_1 \cos\vartheta_1 < -a$$

i.e. when the observer is on the other side of the normal to the plane of the ring through its centre. This is a focal line for the ring source.

In order to clarify what happens when a ray crosses the focal line let us consider the stopping phase for $t \simeq R_2/c$. In this case (2) is given, approximately, by:

$$C_2(t) = \frac{2a}{\sqrt{R_2^2 - R_1^2}} \sqrt{2c/R_2}\, \frac{H(R_2/c - t)}{\sqrt{R_2/c - t}} \tag{7}$$

and using (see Fig. 1)

$$R_2^2 - R_1^2 = 4ar = 4a^2(R_2 \cos \vartheta_2 - 1) \tag{8}$$

we write:

$$C_2(t) = \frac{1}{\sqrt{R_2 \cos \vartheta_2/a - 1}}\, \mathscr{H}[L(t, R_2)] \tag{9}$$

where $\mathscr{H}(L)$ denotes the Hilbert transform of the radiation from a line source (6). Equation (9) is only valid for:

$R_2 \cos \vartheta_2 > a$,

i.e. for waves radiated towards the convex side ($\cos \theta_2 > 0$) of the circular source and which have crossed the focal line.

Thus, the radiation towards the convex side of the ring is of the form $C_1(t)$ before it crosses the focal line and is of the type $C_2(t)$ once it crosses the focal line at F in Fig. 1; i.e. the waveform is Hilbert transformed by the focusing. In the vicinity of the focal line the solutions $C_1(t)$ and $C_2(t)$ are not valid since the term $(R_2^2 - R_1^2)^{-1/2}$ becomes singular.

The term in the square root in front of (5) and (9) is due to geometrical spreading measured from the focal line. In the vicinity of the ring source, R_1 or R_2 are very small and the correction factor is close to one, i.e. near the ring the waves are essentially cylindrical and given by $L(R_1, t)$. In the far field, on the other hand, $R_1, R_2 \gg a$ and the correction factors are of the form $[a/R \cos \theta]^{1/2}$ with $R = R_1$ for the first arrival and $R = R_2$ for the stopping phase. The last one is of course the Hilbert transform of the first.

Neither Madariaga (1977) nor Achenbach & Harris (1978) included Hilbert transformation at the focal line in their analysis of high-frequency radiation, although the latter authors studied the focusing problem. In the frequency domain the absolute spectra of both phases (5) and (9) are the same, but their phases differ by $\pi/2$. The most important effect of the focal line crossing is to be observed in the time domain synthetic accelerograms as will be shown in the next section and is easily seen in the numerical accelerograms calculated by Archuleta & Hartzell (1981) and Campillo (1983) for a buried circular source.

3 Dynamical and quasi-dynamical models of a circular crack

We will apply the geometrical diffraction theory, exposed in the previous section, to the evaluation of the stopping phases from a circular shear fault model. We consider a vertical strike-slip circular fault buried in a homogeneous isotropic elastic half-space. This model was studied by Archuleta & Hartzell (1981) and Campillo (1983) with numerical techniques. The circular fault model was studied also by Madariaga (1976), however his numerical solutions are not very practical for the calculation of near field motions. For this reason, instead of the fully dynamical solution we shall use an approximation to the slip function at the source which retains most of its main characteristics. We follow Boatwright (1980)

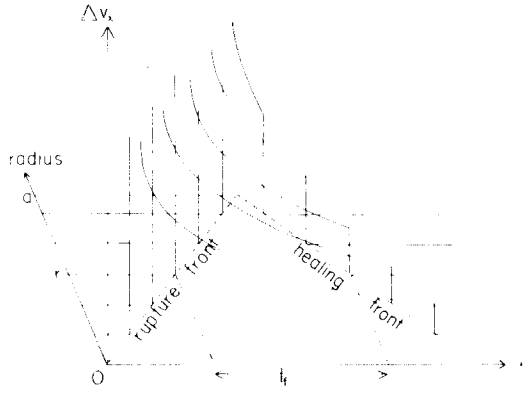

Figure 2. Source time function as a function of radius used in the generation of synthetic accelerograms by Archuleta & Hartzell (1981), Campillo (1984) and in this paper. The rupture front moves at velocity v and the stopping phase propagates at velocity β.

who called such approximations quasi-dynamical. Similar approximations were used by Archuleta & Hartzell (1981) and Campillo (1983) in the numerical calculations which will be used to test our asymptotic results.

The quasi-dynamic slip function we shall use is shown in Fig. 2; it is a truncated version of Kostrov's (1964) solution for a self-similar shear crack that grows with a constant radial velocity v, i.e.

$$\Delta v_x = C(v/\beta)\frac{\sigma_e}{\mu}\beta t\,\frac{H(t - r/v)\,H(t_f - t + r/v)}{\sqrt{t^2 - r^2/v^2}} \tag{10}$$

where Δv_x is the slip velocity which is taken parallel to the x-axis, σ_e is the dynamic stress drop, μ the shear modulus, v the rupture velocity, β the shear wave velocity, t is time measured from the onset of rupture, r is the radius measured from the nucleation point and $H(t)$ denotes the Heaviside function. The rise time t_f is given by:

$$t_f = (1/v + 1/c)(a - r)$$

where a is the final radius of the fault when the rupture suddenly stops. t_f is the time lapse between the beginning of slip at a point with radius r and the arrival of the healing phase radiated by the edge of the fault when it suddenly stops at a circle of radius a. After the arrival of the stopping phase or healing wave (see Fig. 2), slip ceases completely and it stays frozen at this final value. The stopping phase moves inward from the fault edge with a healing velocity c. This model of healing is not exactly what is observed in the numerical solutions of Madariaga (1976) in which P, S and Rayleigh stopping phases are emitted by the edge, but is a close approximation to it if the healing velocity is taken as the shear wave velocity.

The slip velocity (10), although simplified, is still difficult to use to calculate near field accelerograms so that it may only be used in numerical procedures. Let us note, however, that it is strongly concentrated near the rupture front at $r = vt$ where it may be approximately written as:

$$\Delta v_x = C(v/\beta)\frac{\sigma_e}{\mu}\beta\sqrt{r/2v}\,\frac{H(t - r/v)\,H(t_f - t + r/v)}{\sqrt{t - r/v}}. \tag{12}$$

Thus the inverse square root singularity in slip velocity near the rupture front that is typical of all crack models (Freund 1979). In (12) we have kept the healing phase given by $H(t_f - t + r/v)$ because, when r is close to a, the healing phase comes immediately behind the start of slip, i.e. $t_f \to 0$ and it makes an important contribution to the radiation as we shall see below. The slip velocity (12) may be considered as produced by a dislocation of time dependence $t^{-1/2}$ moving with the rupture front. It differs, however, from a classical dislocation model because of the presence of the stopping phase.

4 High-frequency radiation from the circular crack model

In order to approximate the dominating radiation from the circular crack we notice that high frequencies are controlled by the most singular part of the source. This is clearly the abrupt stopping of the rupture at $r = a$. Thus, we make the following hypothesis that we shall verify with the numerical results obtained for the full slip function (10): high-frequency waves are dominated by the stopping phases and these waves may be evaluated by simple asymptotic methods. By high frequencies we mean waves whose wavelength are shorter than the distance to the edge of the fault and than the radius of the source.

From a high-frequency point of view the circular source reduces to a ring that coincides with the final edge of the crack at $r = a$. The radiation from this ring may be calculated by the geometrical methods presented in the previous sections. Referring to Fig. 1, the high-frequency waves come from A_1 – the first stopping phase – and from A_2 – the second one. In order to calculate their amplitude and wave form we proceed in the standard manner of geometrical diffraction theory. We solve first the canonical problem of radiation from a 2-D crack whose edge coincides with the local tangent to the ring $r = a$ at A_1 or A_2. Next, we propagate these canonical waves introducing the geometrical correction included in (5) and for the stopping phase from A_2 the Hilbert transform that appears in (9).

In order to solve the canonical problem we notice that at A_1 and A_2 the slip velocity Δv_x has both an antiplane (screw) and an inplane (edge) component. Radiation from either component may be calculated independently since an antiplane crack generates only *SH*-waves, while *P*- and *SV*-waves are produced by an inplane crack.

Decomposing Δv_x into radial and tangential components we find, respectively:

$$\Delta \dot{u} = V \cos \vartheta \frac{H(t - r/v)\, H(t_f - t + r/v)}{\sqrt{t - r/v}} \tag{13}$$

$$\Delta \dot{v} = V \sin \vartheta \frac{H(t - r/v)\, H(t_f - t + r/v)}{\sqrt{t - r/v}} \tag{14}$$

where:

$$V = C(v/\beta) \frac{\sigma_e}{\mu} \beta \sqrt{r/2v} \tag{15}$$

is the velocity intensity factor and ϕ is the azimuth on the plane measured from the x-axis.

The solution of the canonical problems for the radiation from the vicinity of A_2 and A_1 in the antiplane and plane modes is presented in the Appendix, where it is found by a superposition of dislocations. This method of solution is substantially simpler than the exact solutions for the canonical crack problems developed by Madariaga (1977) and Achenbach & Harris (1978).

For a healing velocity $c = \beta$, one finds for the acceleration pulse radiated by a suddenly stopping antiplane crack with velocity intensity $V \sin \phi$, the following result.

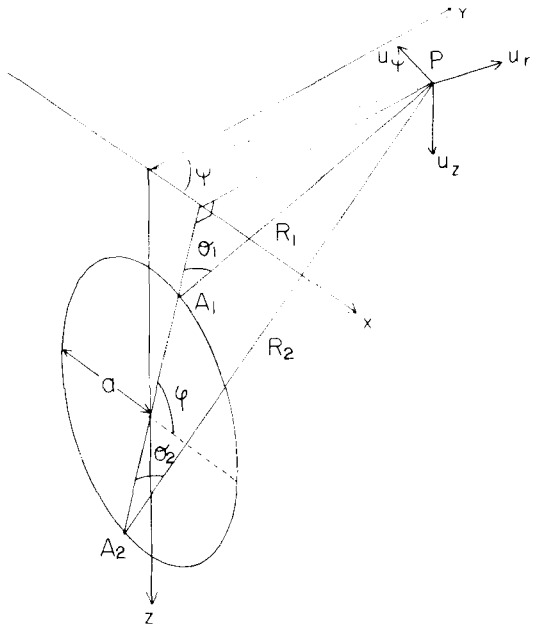

Figure 3. Geometry of the vertical circular fault model used in the calculation of synthetics. The observation point P is on the surface. The radial, transverse and vertical components of acceleration are indicated by the axes drawn at point P.

$$\ddot{u}_{SH}(R_1, \vartheta, \phi) = \frac{V}{2} \sin\phi\, D(v, \beta)\, \frac{v}{1 - v/\beta \cos\vartheta}\, \frac{\sin\vartheta}{\sqrt{2R_1\beta}}\, \delta(t - a/v - R_1/\beta). \tag{16}$$

Similarly for the P-wave radiated by the stopping of a plane crack of velocity intensity $V\cos\phi$ we find:

$$\ddot{u}_P(R_1, \vartheta, \phi) = \frac{V}{2} \cos\vartheta\, \frac{\beta^2}{\alpha^2}\, D(v, \alpha)\, \frac{v}{1 - v/\alpha \cos\vartheta}\, \frac{\sin(2\vartheta)}{\sqrt{2R_1\alpha}}\, \delta(t - a/v - R_1/\alpha), \tag{17}$$

and for the SV-wave:

$$\ddot{u}_{SV}(R_1, \vartheta, \phi) = \frac{V}{2} \cos\vartheta\, D(v, \beta)\, \frac{v}{1 - v/\beta \cos\vartheta}\, \frac{\cos(2\vartheta)}{\sqrt{2R_1\beta}}\, \delta(t - a/v - R_1/\beta) \tag{18}$$

where the factor:

$$D(v, c) = \frac{\sqrt{1/v + 1/c}}{\sqrt{1/\beta + \cos\psi/c}} \tag{19}$$

is due to the effect of the healing phases. These results are proven in the Appendix.

We may now apply the geometrical theory of diffraction to the radiation from the abruptly stopping circular crack. Referring to Fig. 3, at a point P arrive two stopping phases from A_1 and A_2. For the first stopping phase from A_1 the amplitude is modified by the factor $(1 + R_1/a\cos\vartheta_1)^{-1/2}$ in all cases. For the second stopping phase the ray crosses the axial focal line at F (Fig. 1). In this case the second stopping phase suffers

a Hilbert transformation as indicated by (9) and its amplitude has to be modified by: $(R_2/a \cos \vartheta_2 - 1)^{-1/2}$.

For a whole space then the ground acceleration at a point P may be written as:

$$\frac{d^2}{dt^2}\hat{u} = \hat{a}_{P_1}\delta(t - t_{P_1}) - \hat{a}_{P_2}\frac{1}{\pi(t - t_{P_2})} + \hat{a}_{SV_1}\delta(t - t_{S_1}) - \hat{a}_{SV_2}\frac{1}{\pi(t - t_{S_2})} + \hat{a}_{SH_1}\delta(t - t_{S_1}) - \hat{a}_{SH_2}\frac{1}{\pi(t - t_{S_2})} \tag{20}$$

where t_i is the time of propagation for the appropriate wave type from the points A_1 or A_2 to the observation point. The vector amplitudes are given by:

$$\hat{a}_{P_1} = \frac{V}{2}\cos\vartheta\frac{v\beta^2}{\alpha^3}\left(\frac{\alpha a}{2R_1(a + R_1\cos\vartheta_1)}\right)^{1/2}\frac{\sin(2\vartheta_1)}{1 - v/\alpha\cos\vartheta_1}D(v, \alpha)$$

$$\hat{a}_{P_2} = \frac{V}{2}\cos\vartheta\frac{v\beta^2}{\alpha^3}\left(\frac{\alpha a}{2R_2(R_2\cos\vartheta_2 - a)}\right)^{1/2}\frac{\sin(2\vartheta_2)}{1 + v/\alpha\cos\vartheta_2}D(v, \alpha)$$

and similar expressions for $\hat{a}_{SV_1}, \hat{a}_{SV_2}$ . . . derived from (18) and (16).

4.1 ACCELEROGRAMS FOR A VERTICAL CIRCULAR CRACK IN A HALF-SPACE

The accelerations (20) are calculated in a homogeneous medium. They may be used, however, as initial conditions for a ray propagation method. In the application we have in mind here we shall simply assume that the source is buried in a half-space so that the only propagation effect we shall consider is the free surface response. This may be quite complicated because of the S to P conversion at incidence angles greater than critical. The method to calculate the free surface response for incident P-, SV- or SH-waves is well known (Helmberger 1974; Harris & Achenbach 1981) and need not be reproduced here. Let us note that the free surface response to incident SV-waves beyond the critical angle contains a pulse that reproduces that of the incident waves plus its Hilbert transform. Thus on the free surface both the first and the second SV stopping phases will produce a combination of delta-like and $1/t$-like pulses.

5 Comparison with numerical models

In order to test the applicability of the results obtained in the previous section, we will compare our asymptotic solutions with results obtained by numerical integration of a network of point sources distributed on the fault plane. Synthetic accelerograms of this kind have been calculated by Archuleta & Hartzell (1981) and Campillo (1983). It is not possible directly to compare the numerical results with the asymptotic ones because of the finite bandwidth produced by the discretization of the source in the numerical simulations. For this reason, we tried to simulate the synthetic accelerograms convolving our asymptotic results with a low-pass filter.

We will compare our asymptotic accelerograms with those of Campillo (1983) who provided us with a set of synthetics. He used a fully numerical method: the circular source was divided into a network of elementary point sources with an appropriate source time function defined by (10). For each of the point sources, complete accelerograms were calculated by the discrete wavenumber integration method of Bouchon (1979). Finally, the

synthetic records were obtained by superposition of the accelerograms calculated for each point source. Because of the discrete grid path and the discrete integration step of the inverse Fourier transforms there is an upper frequency limit to Campillo's results. He estimates that his results are low pass filtered with a maximum frequency $f_0 = 5$ Hz. This value is also the corner frequency of the two-pole low pass Butterworth filter that Archuleta & Harzell (1981) applied twice to their accelerograms in order to reduce numerical noise.

We also filtered our solutions with a low pass box-car filter with a cut-off frequency of 5 Hz. In this case the delta function in (20) becomes:

$$\delta(t) \to 2f_0 \frac{\sin(2\pi f_0 t)}{2\pi f_0 t} \tag{21}$$

with a peak value at $t = 0$ of $2f_0 = 10$. Similarly the $(\pi t)^{-1}$ pulse in (20) is modified into:

$$\frac{1}{\pi t} \to 2f_0 \left[\frac{\cos(2\pi f_0 t) - 1}{2\pi f_0 t}\right] \tag{22}$$

with a peak value of $1.45 f_0 = 7.25$ at $t = \pm 0.375/f_0$. These low-pass filters were designed in order to approximate the nominal cut-off frequencies of the synthetics calculated by Campillo (1983). In fact, the effective low-frequency cut-off of his numerical scheme is probably lower than 5 Hz; this makes it difficult to compare these amplitudes and those calculated by us.

The geometry of the source model is shown in Fig. 3. For the comparison we use Campillo's (1983) values: radius $a = 5$ km, hypocentral depth at 7 km, rupture velocity $v = 0.9\beta$. The velocity intensity V in (15) was calculated using Archuleta & Hartzell's (1981) parameters: $\sigma_e = 100$ bar, $\mu = 3 \times 10^5$ bar and $C(v/\beta) = 1$. These were also used by Campillo (1983). The homogeneous elastic half-space has a shear wave velocity $\beta = 3$ km s^{-1} and a P-wave velocity $\alpha = 5.2$ km s^{-1}. For the synthetic and asymptotic results compared in Fig. 4 we took the observer at a distance $D = 6$ km from the origin and at angles of 30° and 60° with respect to the x-axis.

In Fig. 4 (upper) we plot the three components of accelerations at 30° and (lower) those for 60°. The numerical calculations are shown at the bottom of each row with the asymptotic ones above them. On the record at the bottom right hand corner we indicate the dominating phases. P_0, S_0 are the P and S initial phases radiated from the hypocentre. P_1, S_1 and P_2, S_2 are the P- and S-wave stopping phases from the nearest (1) and furthest (2) points on the source edge. In our synthetics we did not include the initial phases P_0, S_0; only stopping phases were calculated. The coincidence of the arrival time and the similarity of the numerical and asymptotic waveforms is striking. This demonstrates our main contention that at high frequencies the radiation from most of the fault interferes destructively, only the radiation from the fault edge contributes significantly to the accelerograms. The delta-like and t^{-1}-like pulses are clearly identified in most of the records. Nevertheless, some differences appear. In part they are due to the neglect of the starting phases in our asymptotics, and also to the clear difference in frequency content between our asymptotics and the numerical scheme used by Campillo is probably lower than 5 Hz. This affects the amplitudes and we observe that the synthetics have almost twice the amplitude of the numerical results. A better compromise would be to assume that Campillo's results are effectively filtered by the numerical method at 2.5–3 Hz. This is not of much geophysical interest since the acceleration amplitudes are clearly controlled by the artificial cut-off frequency. A more physical approach would be to limit the high frequencies with an attenuation filter; this will be done in the next section.

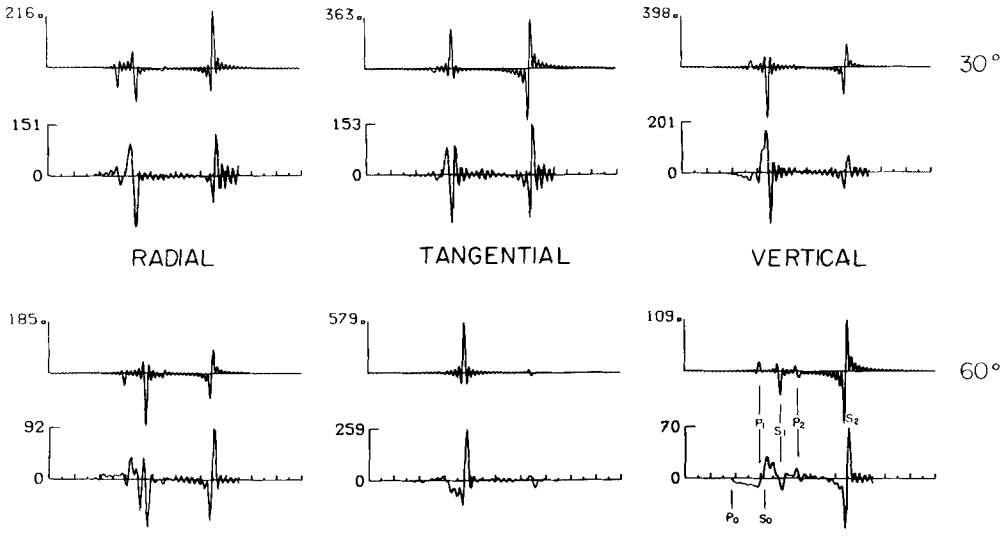

Figure 4. Comparison between the numerical simulations by Campillo (1984) and the asymptotic accelerograms calculated by our method. Two sets of accelerograms were calculated at a distance of 6 km and angles of 30° (top) and 60° (bottom) from the origin. The asymptotics are shown immediately above the synthetics. The numbers next to the vertical axis indicate the amplitude of the traces.

6 Asymptotic accelerograms in a dissipative medium

The theoretical results (20) predict infinite amplitudes for the acceleration pulses associated with the stopping phases. This corresponds to a flat (white) acceleration spectrum at high frequencies. In the Earth the high frequencies will be attenuated and filtered by a number of source and propagation processes that are collectively described by f_{max}, the high frequency acceleration cut-off frequency discussed by Hanks (1982). The physical origin of f_{max} is the subject of much current discussion (Papageorgiou & Aki 1983; Hanks 1982). As noted by these authors the f_{max} cut-off is very sharp so that in the following examples we shall simulate its effect by an effective attenuation (Q-value) along the ray trajectory. The delta-like impulse is replaced by the attenuation operator whose Fourier transform is given by:

$$F(\omega, T/Q) = \exp\left[-\omega T/2Q + i\frac{\omega T}{\pi Q}\log(\omega/\omega_0)\right]. \tag{23}$$

T is the travel time, Q the quality factor and $\omega_0 = 2\pi f_0$ is the reference frequency (Carpenter 1967). The Hilbert transform of this pulse was calculated also in the frequency domain. The synthetic accelerograms were finally calculated by inversion of the transform to the time domain.

We calculated synthetic accelerograms for the same source geometry as described in Fig. 3 with parameters $R = 5$ km, $H = 7$ km, $\upsilon = 0.9\beta$, $\sigma_e = 100$ bar. The elastic velocities were $\alpha = 5.2\,\mathrm{km\,s^{-1}}$, $\beta = 3\,\mathrm{km\,s^{-1}}$ and the equivalent quality factor was taken as $Q = 50$. Three profiles were calculated so that the variety of waveforms associated with this overly simplified source model may be appreciated. The position of the profiles with respect to the source is described in Fig. 5 where the dots indicate the points where the asymptotic accelerograms were generated.

Fig. 6 shows the accelerograms calculated at a radial distance of 6 km from the origin

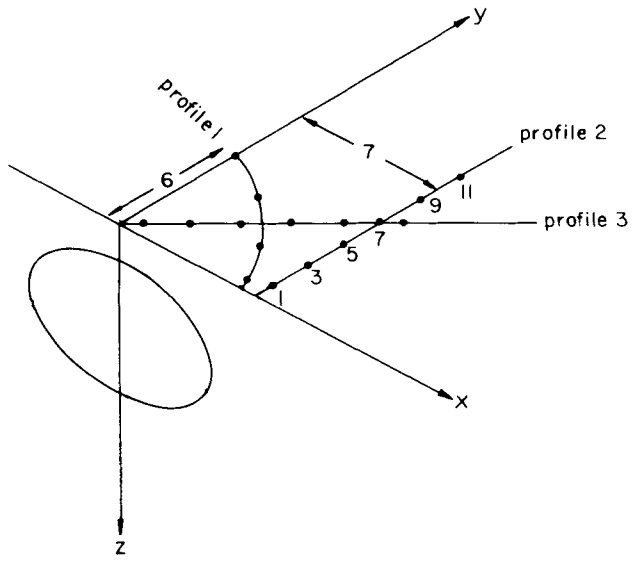

Figure 5. Position of the profiles calculated in Figs 6–8. Profile 1 is at a radius of 6 km from the origin. Profile 2 is a straight line at an angle of 45° with respect to x. Profile 3 is perpendicular to the x-axis at $x = 7$ km.

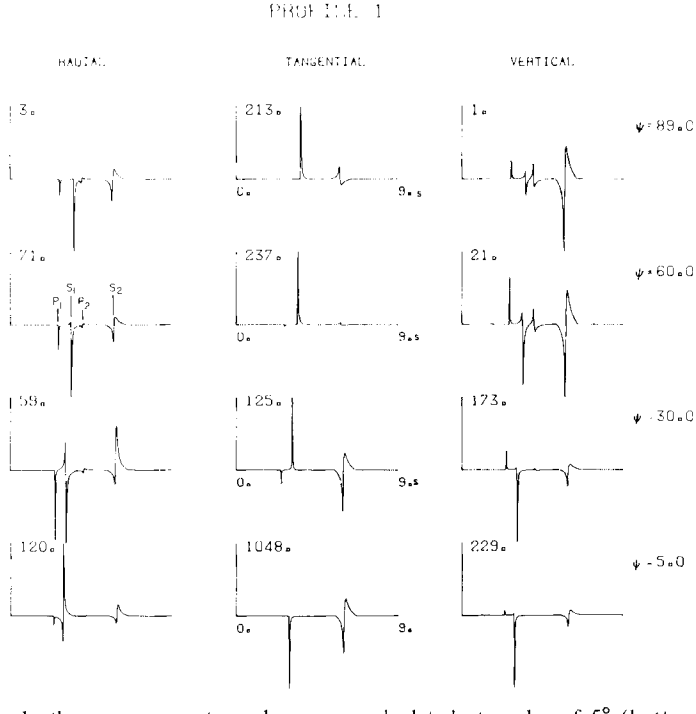

Figure 6. Profile 1: three component accelerograms calculated at angles of 5° (bottom), 30°, 60° and 90° (top) with respect to the x-axis. Values next to vertical axes indicate the maximum acceleration in cm s^{-2}.

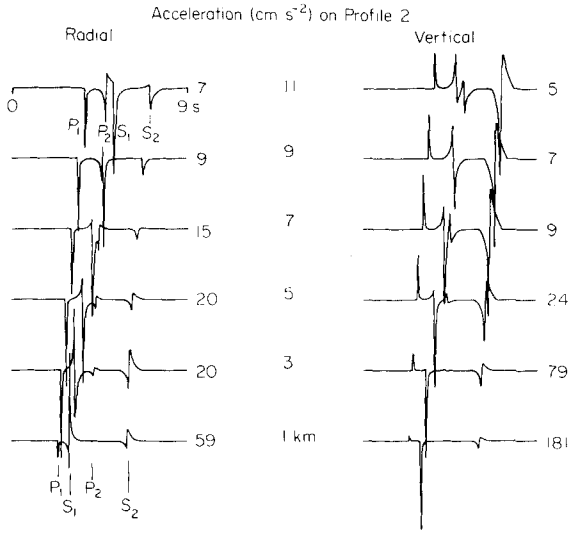

Figure 7. Profile 2: linear profile at an angle of 45° with respect to the x-axis. Numbers at the end of each record indicate the maximum acceleration in cm s^{-2}. Only radial and vertical components are shown.

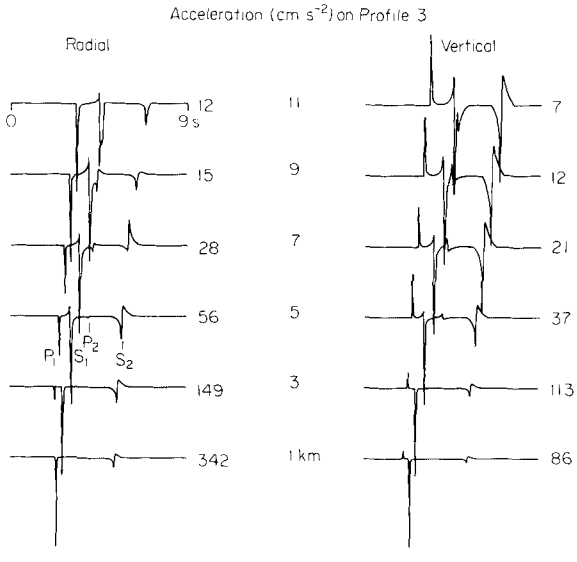

Figure 8. Profile 3: linear profile along a line perpendicular to the x-axis. The numbers at the end of each trace indicate the maximum accelerations in cm s^{-2}. Only radial and vertical acceleration are shown.

and at azimuths of 5°, 30°, 60° and 90°. The asymptotic results at 30° and 60° may be compared with those shown in Fig. 4 and which were calculated at the same places and filtered in order to simulate Campillo's (1983) results. At the azimuth $\theta = 90°$ both P- and SV-waves are on a nodal plane while SH is at a maximum of its radiation pattern; this explains why the radial and vertical components are zero for this angle. The very large amplitude at $\theta = 5°$ are due to the directivity effects of the high rupture velocity (90 per cent of the shear wave velocity). It is clearly seen in these asymptotic accelerograms that the first S-stopping phase (S_1) dominates the records.

In Fig. 7 we show the asymptotic accelerograms along profile 2 in Fig. 5. The calculation points are situated along a line perpendicular to the x-axis 7 km from the origin. The maximum acceleration decreases very rapidly with distance from the fault plane – this decrease is faster than one over the distance to the fault because of the effect of attenuation on the accelerograms. Between 5 and 7 km the second P stopping phase crosses over the first S stopping phase – this produces most of the complexity in those asymptotic accelerograms. Finally in Fig. 8 we show the results along profile 3 where most of its characteristics are similar to those observed on profile 2.

7 Conclusions

This paper is part of a project to develop asymptotic methods for the calculation of near field accelerograms. It is based upon the observation that the main source of radiation during shear fracture is the stress and slip velocity concentrations near the rupture front. These concentrations are characteristic of all crack and dislocation solutions. The strongest radiation occurs when the rupture front rapidly decelerates or enters a zone of rapidly varying stress or strength conditions. In the particular case studied in this paper we reconsider the simple circular crack model that grows at a constant rupture velocity until it abruptly stops. This model was solved by Madariaga (1976) for the slip velocity on the crack and for the radiation in the near field. Using an approximation to the slip function, Archuleta & Hartzell (1981) studied its near field. In this paper we showed that the strong motion records will be dominated by the stopping phases and we proposed a simple way to calculate them asymptotically. Two important changes with respect to Achenbach & Harris (1978) and Madariaga (1977) were introduced. First, the effect of focusing is re-evaluated showing that a phase shift (Hilbert transformation) is produced when the rays cross the axis of the circular fault. Second, a simpler approximation is proposed for the calculation of the radiation pattern due to a rupture front that suddenly accelerates or decelerates. This is obtained by means of dislocation approximations to the crack solutions. The advantage of this formulation is that it may be easily extended to the more realistic problem where fracture arrest does not occur simultaneously around the fault edge. Once this problem is solved, it will be possible to tackle realistic problems where the high-frequency radiation is due to the interaction of an arbitrarily shaped rupture front with barriers and asperities of general geometry. The complete solution of this problem by means of asymptotic methods requires that the canonical solutions for the interaction of a rupture front and stress and strength heterogeneities be solved. Some of the results of this work will be reported in the future (Bernard & Madariaga 1984).

Acknowledgments

We thank M. Bouchon and M. Campillo for many useful discussions. R. Archuleta provided a thorough and enlightening review.

This work was sponsored by the Institut National d'Astronomie et de Géophysique (INAG) under its programme ATP Sismogenèse. P. Bernard has been supported by the Bureau de Recherches Géologiques et Minières (BRGM). Institut de Physique du Globe, contribution no. 686.

References

Achenbach, J. D. & Harris, J. A., 1978. Ray methods for elastodynamic radiation from a slip zone of arbitrary shape, *J. geophys. Res.*, **83**, 2283–2291.

Archuleta, R. J. & Hartzell, S. H., 1981. Effects of fault finiteness on near-source ground motion, *Bull. seism. Soc. Am.*, **71**, 939–957.

Bernard, P. & Madariaga, R., 1984. A new asymptotic method for the modelling of near field accelerograms, *Bull. seism. Soc. Am.*, in press.

Boatwright, J., 1980. A spectral theory for circular seismic sources; simple estimates of source dimensions, dynamic stress drop and radiated energy, *Bull. seism. Soc. Am.*, **70**, 1–27.

Bouchon, M., 1979. Discrete wave number representation of elastic waves in three-space dimensions, *J. geophys. Res.*, **84**, 3609–3614.

Campillo, M., 1984. Numerical evaluation of the near field high-frequency radiation from quasi-dynamic circular faults, *Bull. seism. Soc. Am.*, **73**, 723–734.

Carpenter, E. W., 1967. Teleseismic signals calculated from underground, underwater and atmospheric explosions, *Geophysics*, **32**, 17–32.

Copson, E. T., 1967. *Asymptotic Expansions*, Cambridge University Press.

Freund, L. B., 1972. Crack propagation in an elastic solid subject to general loading. II. Non-uniform rate of extension, *J. mech. Phys. Solids*, **20**, 141–152.

Feund, L. B., 1979. The mechanics of dynamic shear crack propagation, *J. geophys. Res.*, **84**, 2199–2209.

Hanks, T. C., 1982. F_{max}, *Bull. seism. Soc. Am.*, **72**, 1867–1879.

Harris, J. G. & Achenbach, J. D., 1981. Near-field surface motions excited by radiation from a slip zone of arbitrary shape, *J. geophys. Res.*, **86**, 9352–9356.

Hartzell, S. & Helmberger, D. V., 1982. Strong-motion modeling of the Imperial Valley earthquake of 1979, *Bull. seism. Soc. Am.*, **72**, 571-596.

Heaton, T. H. & Helmberger, D. V., 1979. Generalized ray models of the San Fernando earthquake, *Bull. seism. Soc. Am.*, **69**, 1311–1341.

Helmberger, D. V., 1974. Generalized ray theory for shear dislocations, *Bull. seism. Soc. Am.*, **64**, 45–64.

Keller, J. B., 1962. Geometrical theory of diffraction, *J. opt. Soc. Am.*, **52**, 116–130.

Kostrov, B. V., 1964. Self-similar problems of propagation of shear cracks, *J. appl. Math. Mech.*, **28**, 1077–1087.

Kostrov, B. V., 1975. On the crack propagation with variable velocity, *Int. J. Fracture Mech.*, **14**, 47–56.

Madariaga, R., 1976. Dynamics of an expanding circular fault, *Bull. seism. Soc. Am.*, **65**, 163–182.

Madariaga, R., 1977. High-frequency radiation from crack (stress drop) models of earthquake faulting, *Geophys. J. R. astr. Soc.*, **51**, 625–651.

Madariaga, R., 1983. High-frequency radiation from dynamic earthquake fault models, *Annls Geophys.*, **1**, 17–24.

Papageorgiou, A. J. & Aki, K., 1983. A specific barrier model for the quantitative description of inhomogeneous faulting and the prediction of strong ground motion. II. Applications of the model, *Bull. seism. Soc. Am.*, **73**, 953–978.

Rose, L. R. F., 1976. An approximate (Wiener-Hopf) kernel for dynamic crack problems in linear elasticity and viscoelasticity, *Proc. R. Soc. A*, **349**, 497–521.

Appendix

The canonical problems for the radiation of stopping phases from a sudden change in the rupture velocity of a plane or antiplane crack were solved exactly by Madariaga (1977) using the techniques developed by Kostrov (1975); and, independently, by Achenbach & Harris (1978) using Freund's (1972) method. Although their results were expressed in closed form, they are quite complicated to calculate because of the presence of a function derived from Rayleigh's denominator. An examination of these solutions shows that the complications arise because of the presence of healing waves that are radiated into the crack when the rupture front accelerates or decelerates. These stopping phases include Rayleigh waves which are the source of the complexity. Rose (1976) showed that one could get a very good approximation if Rayleigh's quotient was replaced by a simpler expression. We have found that this is equivalent to assuming that once the crack stops a simple healing wave of velocity c close to β propagates inside the crack. After the passage of this healing wave slip ceases

completely. This is actually the approximation (10) adopted by Boatwright (1981), Archuleta & Hartzell (1981) and Campillo (1983) in their quasi-dynamic approximations of the circular shear crack. Thus the approximation (10) has the double interest that it simplifies the canonical problem, and that it corresponds to the approximate models used to calculate numerical accelerograms by the above mentioned authors.

Let us consider the antiplane problem. An infinite screw dislocation line parallel to $\hat{e}_y$ appears on the $z = 0$ plane at $x = \xi$. The slip velocity produced by this dislocation is:

$$\Delta\dot{v}(x, z, t) = \delta(t)\,\delta(x - \xi)\,\hat{e}_y. \tag{A1}$$

The displacement field radiated by it is:

$$v_0(x, z, t; \xi) = \frac{1}{2\pi}\frac{t}{r}\frac{\sin\vartheta}{\sqrt{t^2 - r^2/\beta^2}}H(t - r/\beta) \tag{A2}$$

where r, θ are radial coordinates of (x, z) with respect to $(\xi, 0)$ and β is the shear wave velocity.

If the slip velocity for this dislocation line is changed from $\delta(t)$ into:

$$D(t, \xi) = V\frac{H(t - \xi/v)\,H(t_f - t + \xi/v)}{\sqrt{t - \xi/v}} \tag{A3}$$

where:

$$t_f = \left(\frac{1}{v} + \frac{1}{c}\right)(a - \xi) \tag{A4}$$

we obtain the slip function (13–14) at one point on the fault. The displacement at (r, θ) is simply the convolution of (A3) with (A2). Consider now a continuous distribution of dislocations of time function (A3) distributed on $0 < \xi < a$. In this case the slip velocity on the fault plane becomes:

$$\Delta v(x, t) = V\frac{H(t - \xi/v)\,H(t_f - t + \xi/v)}{\sqrt{t - \xi/v}}H(a - \xi) \tag{A5}$$

which is identical to the approximations (13) and (14) for the slip velocity on a crack. The displacement field generated by the dislocation distribution (A5) is:

$$v(r, \vartheta, t) = \int^a D(t, \xi) * v_0(x, z, t; \xi)\,d\xi. \tag{A6}$$

where the asterisk indicates convolution in time. The lower limit is left undefined on purpose since we are interested here in the radiation from the vicinity of a. The convolution (A6) may be easily calculated in the frequency domain. Let $\tilde{v}$ be the Fourier transform of (A6), then

$$\tilde{v}(r, \vartheta, \omega) = \int^a \tilde{D}(\omega, \xi)\,\tilde{v}_0(x, z, \omega; \xi)\,d\xi \tag{A7}$$

where:

$$\tilde{D}(\omega, \xi) = V\exp(-i\omega\xi/v)\int_0^{t_f}\frac{\exp(-i\omega t)}{\sqrt{t}}\,dt. \tag{A8}$$

For $\tilde{v}_0$ we use the high-frequency approximation to the transform of (A2):

$$\tilde{v}_0(x, z, \omega; \xi) = \frac{1}{2\pi}\frac{\sin v}{\sqrt{2r\beta}}\sqrt{\frac{\pi}{i\omega}}\exp(-i\omega r/\beta). \tag{A9}$$

Reinserting (A8) and (A9) into (A7) we find:

$$\tilde{v}(r, \vartheta, \omega) = \frac{V}{2\pi}\frac{\pi}{2i\omega\beta}\int^a d\xi \frac{\sin\vartheta}{\sqrt{r}}\exp[-i\omega(r/\beta + \xi/v)]\int_0^{t_f}\frac{\exp(-i\omega t)}{\sqrt{t}}dt. \tag{A10}$$

This integral may be evaluated at high frequencies noting that the dominant part of the radiation comes from the vicinity of $\xi = a$. We then make the following approximations:

(1) $\sin\theta r^{-1/2}$ is evaluated at $\xi = a$, otherwise it is independent of ξ. (2) $r = r_0 + (a - \xi)\cos\vartheta$ where r_0 is the radial distance to the observer from the edge of the crack at $\xi = a$. Then

$$\tilde{v}(r, \vartheta, \omega) = \frac{V}{2\pi}\sqrt{\frac{\pi}{i\omega}}\exp[-i\omega(r_0/\beta + a/v)]\frac{\sin\vartheta}{\sqrt{2r_0\beta}}I(r, \vartheta, \omega) \tag{A11}$$

where:

$$I(r, \vartheta, \omega) = \int^a d\xi \exp\|i\omega(a - \xi)/v[1 - v/\beta\cos\vartheta]\|\int_0^{t_f}\frac{\exp(-i\omega t)}{\sqrt{t}}dt \tag{A12}$$

has to be evaluated as $\omega \to \infty$. Integrating by parts we find:

$$I = -\frac{v(1/v + 1/c)^{1/2}}{i\omega[1 - v/\beta\cos\vartheta]}\int^a d\xi \frac{\exp[-i\omega(a - \xi)(1/c + 1/\beta\cos\vartheta)]}{\sqrt{a - \xi}}$$

and, finally, this integral is dominated by the singularity near $\xi = a$. Then (Copson 1967, p. 23).

$$I \simeq \frac{v\sqrt{\pi}}{i\omega\sqrt{i\omega}}\frac{\sqrt{1/v + 1/c}}{\sqrt{1/c + 1/\beta\cos\vartheta}}\frac{1}{[1 - v/\beta\cos\vartheta]} \tag{A13}$$

Inserting in (A11) we finally find:

$$-\omega^2\tilde{v}(r, \vartheta, \omega) = \frac{V}{2}D(v, c)\frac{v}{1 - v/\beta\cos\vartheta}\frac{\sin\vartheta}{\sqrt{2r_0\beta}}\exp[-i\omega(r_0/\beta + a/v)] \tag{A14}$$

where:

$$D(v, c) = \frac{\sqrt{1/v + 1/c}}{\sqrt{1/c + 1/\beta\cos\vartheta}} \tag{A15}$$

is a correction factor due to the finite healing velocity c. Inverting to the time domain we obtain the acceleration pulses:

$$\ddot{v}(r, \vartheta, t) = \frac{V}{2}D(v, c)\frac{v}{1 - v/\beta\cos\vartheta}\frac{\sin\vartheta}{\sqrt{2r\beta}}\delta(t - r_0/\beta - a/v). \tag{A16}$$

Note that when $\cos\vartheta > -\beta/c$ the coefficient D becomes imaginary and the delta pulse in (A16) has to be Hilbert transformed. In this paper we take $c = \beta$ so that this situation does not arise.

Using the same procedure for a plane crack one finds that SV-waves are given also by (A16) but with the radiation pattern $\sin\theta$ replaced by $\cos 2\theta$. For P-waves the time dependence is the same but the amplitude changes to:

$$\ddot{v}(r, \vartheta, t) = \frac{V}{2}\frac{\beta^2}{\alpha^2} D(v, c) \frac{v}{1 - v/\alpha \cos\vartheta} \frac{\sin 2\theta}{\sqrt{2r_0\alpha}} \delta(t - r_0/\alpha - a/v).$$

In $D(r, c)$ given by (A15) β has to be replaced by α.